Structures of LaH_{10}, EuH_9, and UH_8 superhydrides rationalized by electron counting and Jahn-Teller distortions in a covalent cluster model

Harry W. T. Morgan* and Anastassia N. Alexandrova

Department of Chemistry and Biochemistry, University of California, Los Angeles, Los Angeles, California 90095-1569, United States

E-mail: harrywtmorgan@g.ucla.edu

Structural optimizations of $[EuH_9]^-$ and $[LaH_{10}]^+$

To test our theory that the bond-compression distortion in EuH_9 is driven by the electron count of the H_8 cluster, we optimized the structures of $[EuH_9]^-$ and $[LaH_{10}]^+$. The optimizations were performed at 150 GPa with a uniform background charge to compensate the added/removed electrons, using the NELECT method in VASP. According to our theory, if $[LaH_{10}]^+$ has only two electrons on H_8 then it should be susceptible to the same Jahn-Teller distortion as EuH_{10} and should undergo axial compression, while if $[EuH_9]^-$ has three electrons on H_8 then all the H-H bond lengths in the cluster should be equal. The optimized structure of $[LaH_{10}]^+$ is as predicted - the H_8 cluster is compressed in one direction, to a similar extent as in EuH_{10}. However, the optimized structure of $[EuH_9]^-$ has the same distortion pattern as EuH_9, with bond lengths and angles distorted, and the same structure is reached whether the initial structure is distorted EuH_9 or more symmetrical LaH_9 (which

has angle distortions only). We suspect that these charged systems are not well behaved because of the substantial uniform background charge - one electron per formula unit must be added or removed, and the calculations were performed at a pressure of 150 GPa where the lattices are significantly compressed. For $[EuH_9]^-$ this is likely to lead to delocalization of the added electrons, due to the uniform positive charge, in which case it is not localized on H_8 and will not remove the Jahn-Teller instability.

Supplementary figures

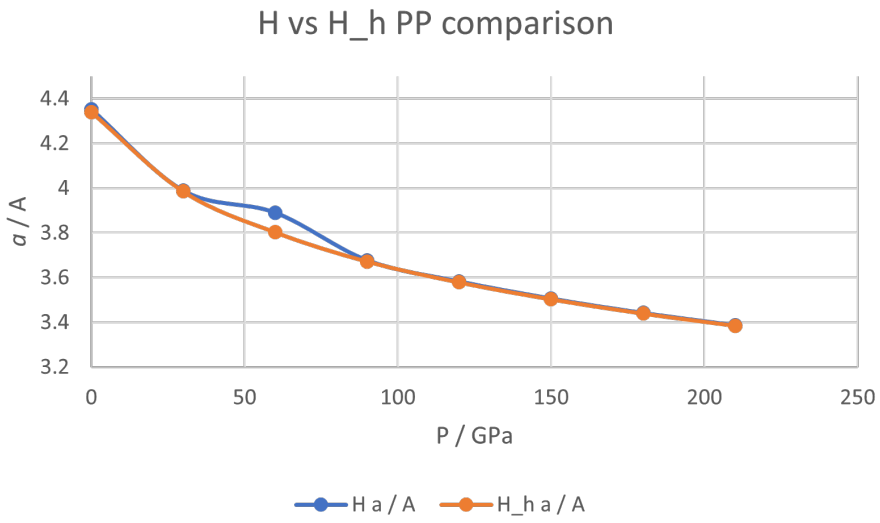

Figure S1: Optimized lattice parameter a for CaH_6 vs pressure with the standard ("H", blue) and hard ("H_h", orange) pseudopotentials from the VASP PAW-PBE library.

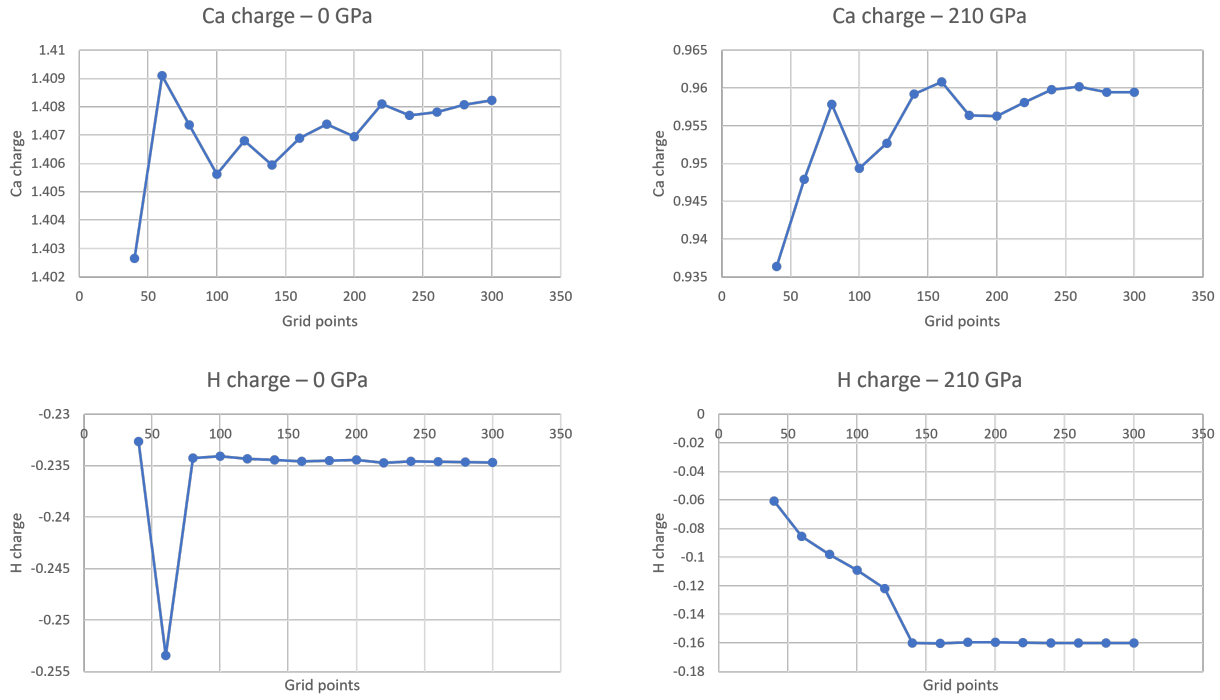

Figure S2: QTAIM atomic charges for CaH_6 at 0 and 210 GPa as a function of NG(X,Y,Z)F, the number of points in the fine FFT grid.

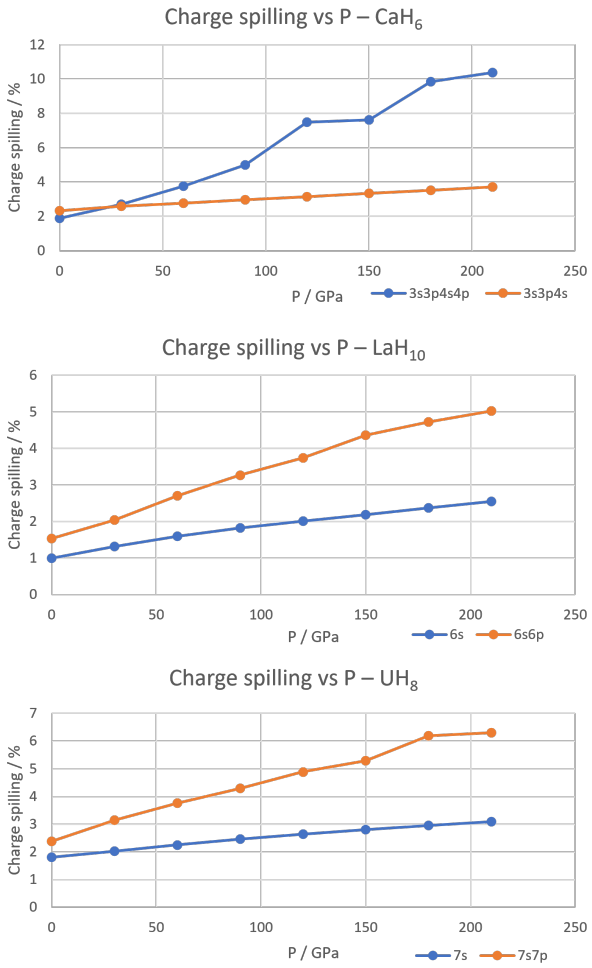

Figure S3: Charge spilling (%) vs P (GPa) of LOBSTER projections of CaH_6, LaH_{10}, and UH_8 with and without unoccupied p orbitals on the metal (blue and orange, respectively)

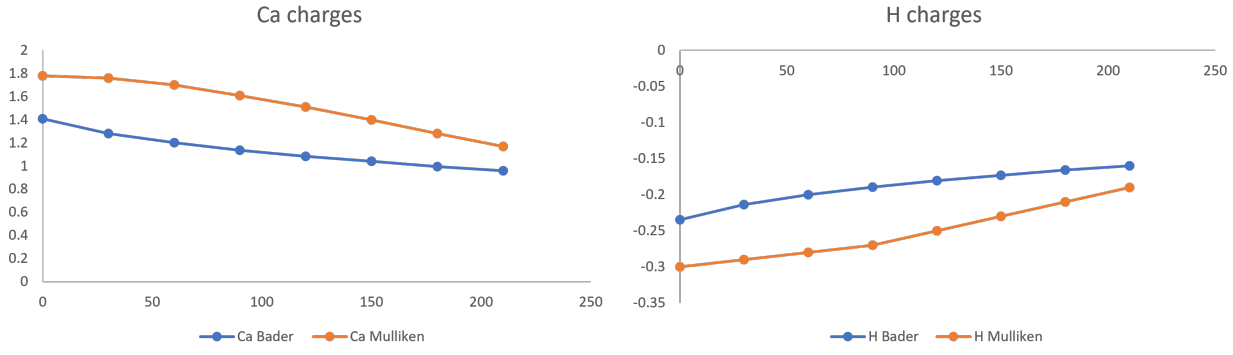

Figure S4: Atomic charges vs pressure (GPa) for CaH_6 using the Bader (blue) and Mulliken (orange) methods.

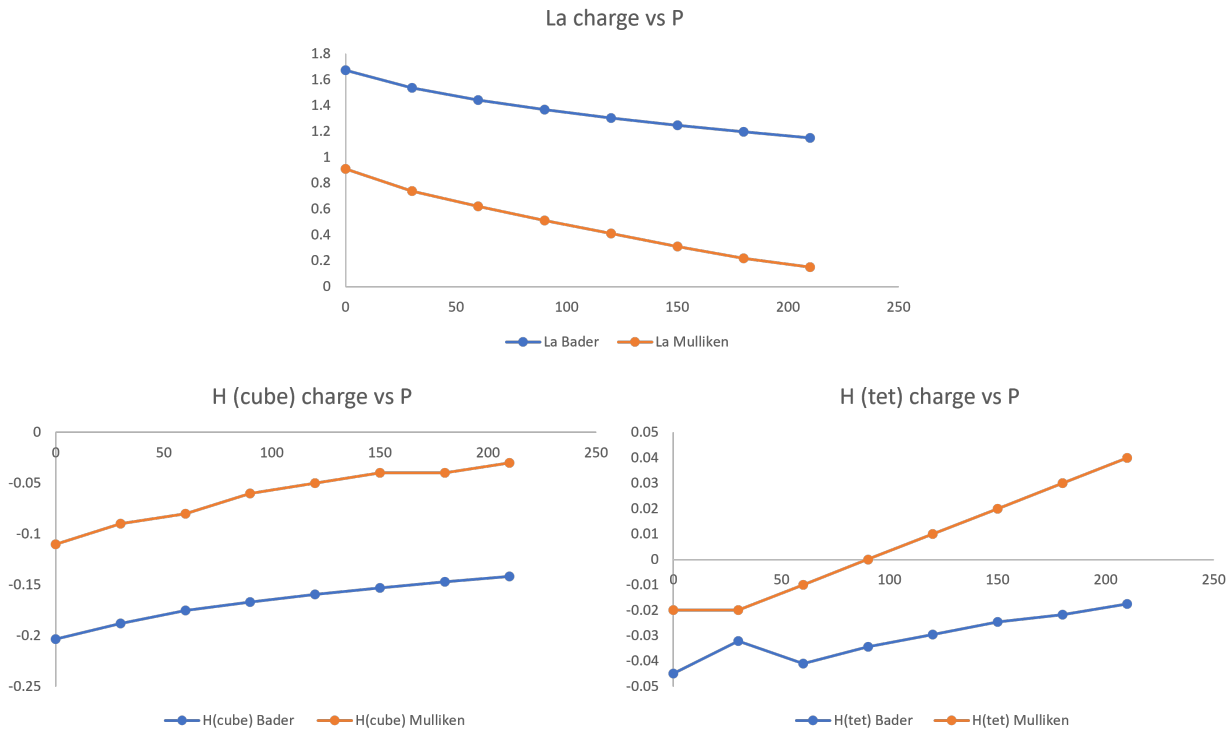

Figure S5: Atomic charges vs pressure (GPa) for LaH_{10} using the Bader (blue) and Mulliken (orange) methods.

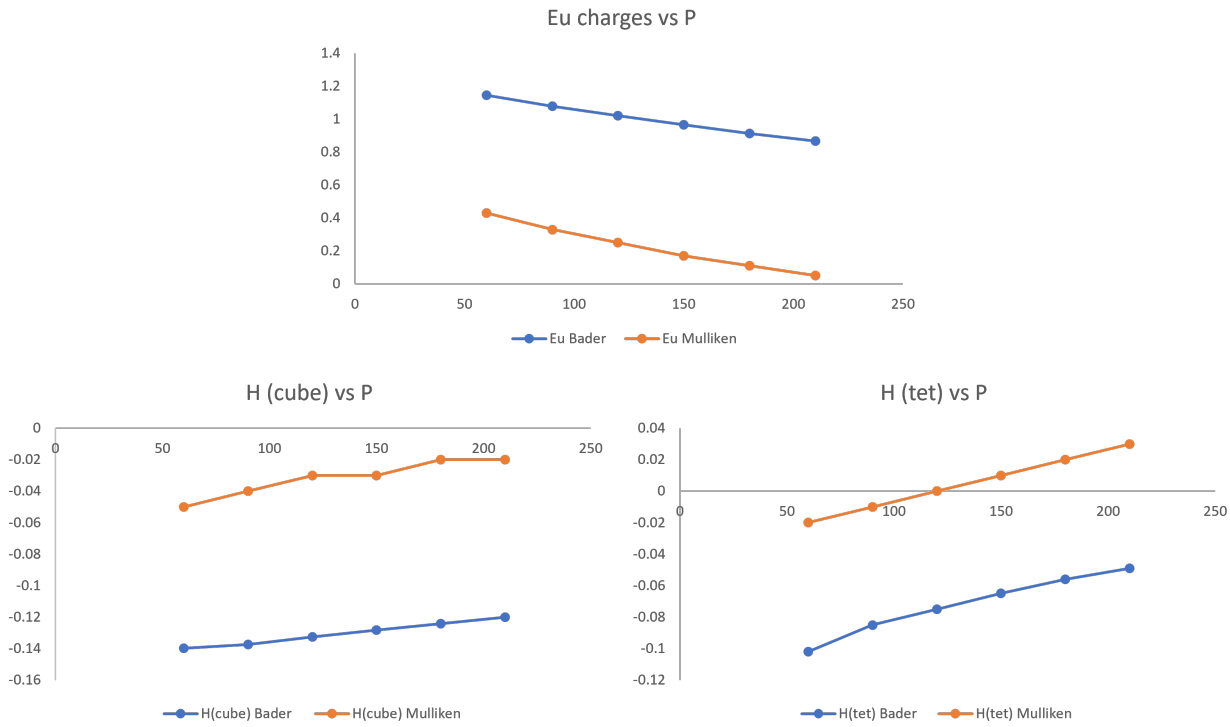

Figure S6: Atomic charges vs pressure (GPa) for EuH_9 using the Bader (blue) and Mulliken (orange) methods.

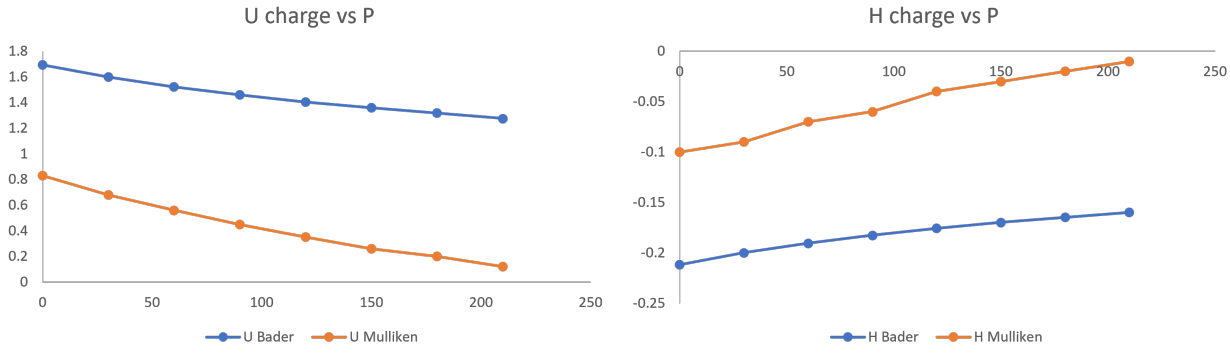

Figure S7: Atomic charges vs pressure (GPa) for UH_8 using the Bader (blue) and Mulliken (orange) methods.

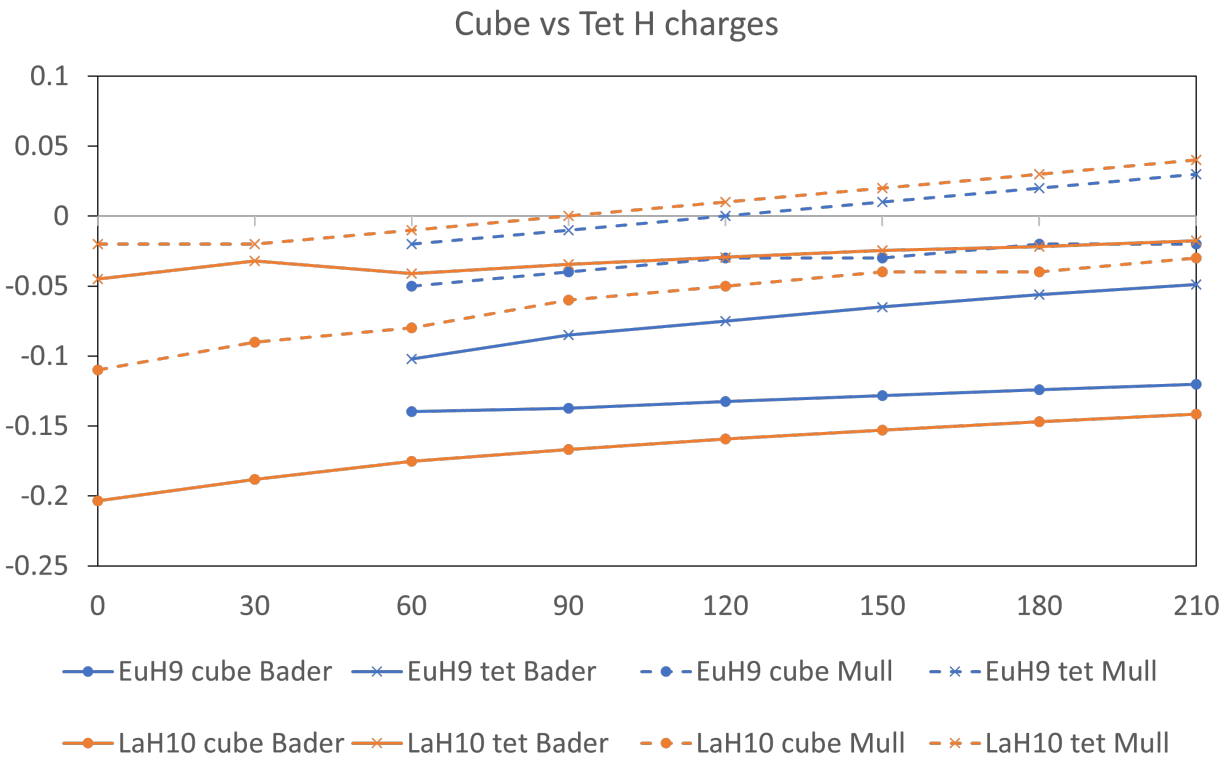

Figure S8: Atomic charges for hydrogen in cube (circles) and tetrahedral (crosses) sites for EuH_9 (blue) and LaH_{10} (orange) using Bader (solid lines) and Mulliken (dashed lines) analysis.

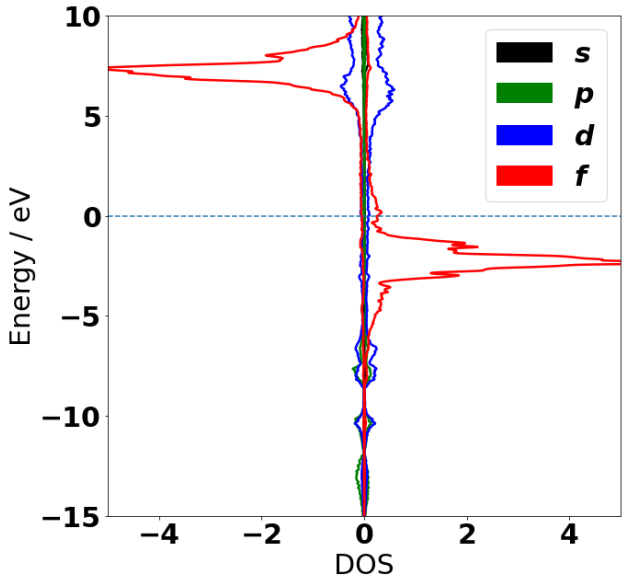

Figure S9: Projected density of states for Eu in EuH_9 at 150 GPa. *s* states are shown by the black curve, *p* by green, *d* by blue, and *f* by red. The spin-up channel is denoted by positive DOS values and the spin-down channel by negative DOS. The Fermi energy is set to 0 on the energy scale.

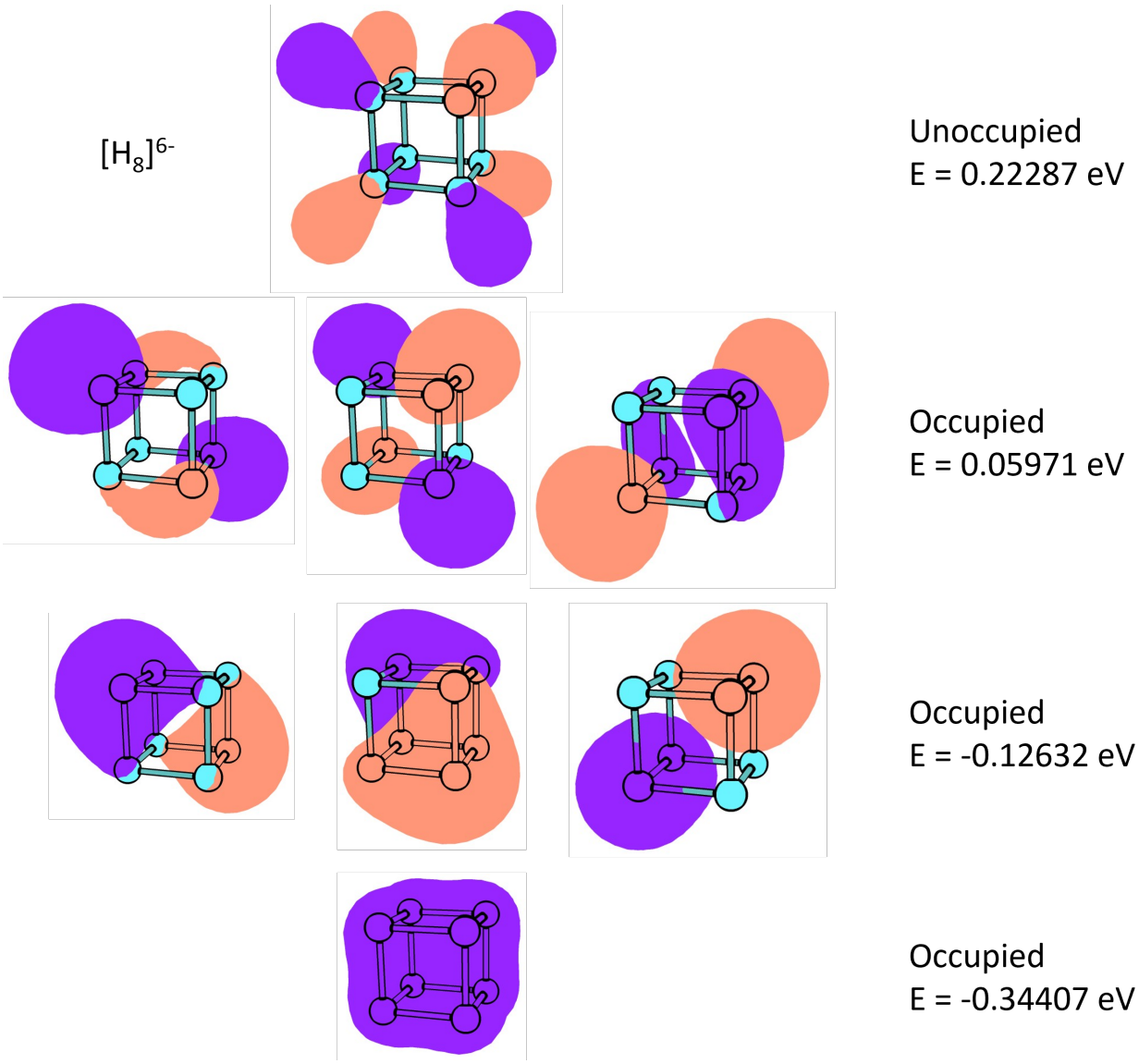

Figure S10: Calculated molecular orbitals for $[H_8]^{6-}$ using the geometry from the optimized structure of UH_8 at 150 GPa.

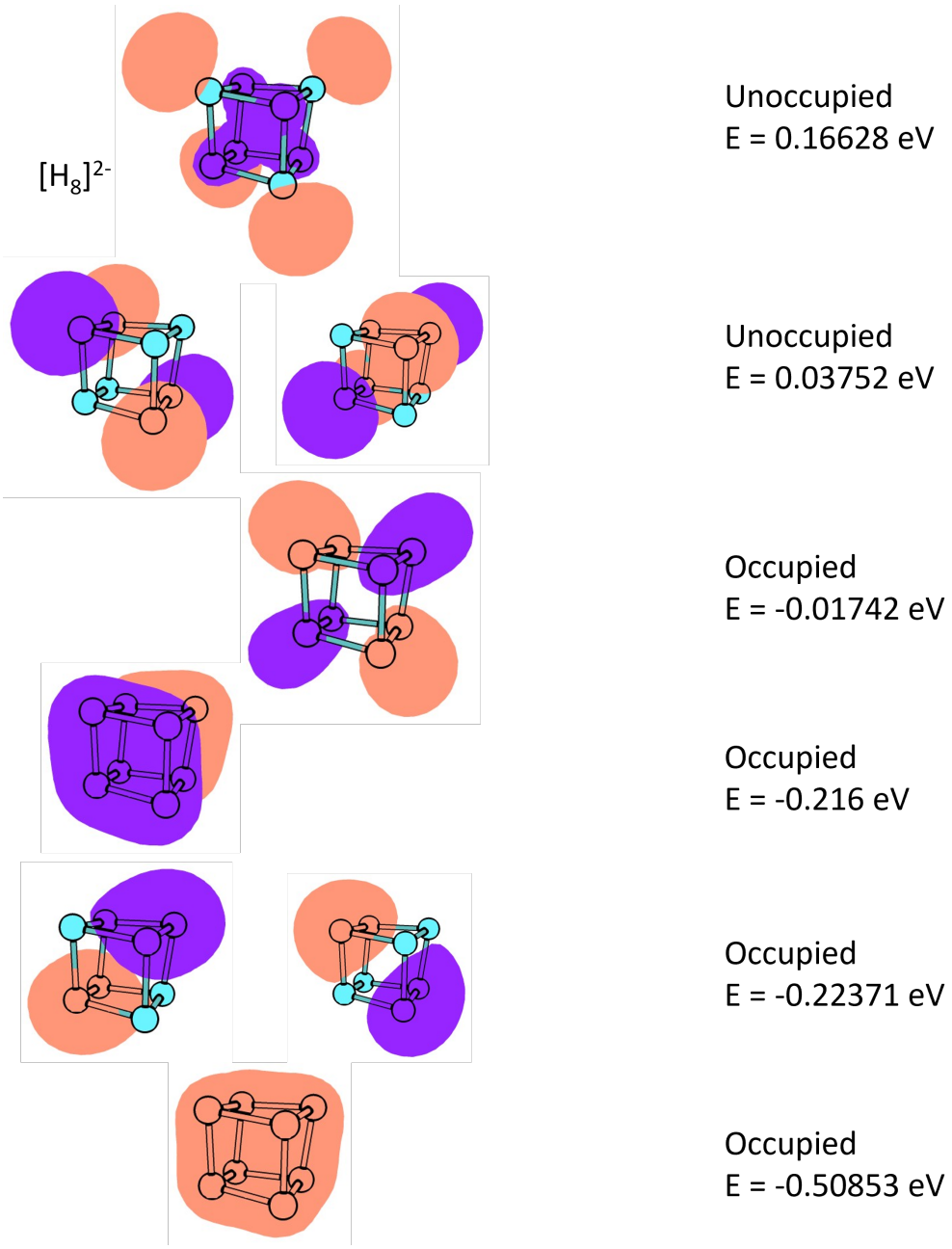

Figure S11: Calculated molecular orbitals for $[H_8]^{2-}$ using the geometry from the optimized structure of EuH_9 at 150 GPa.

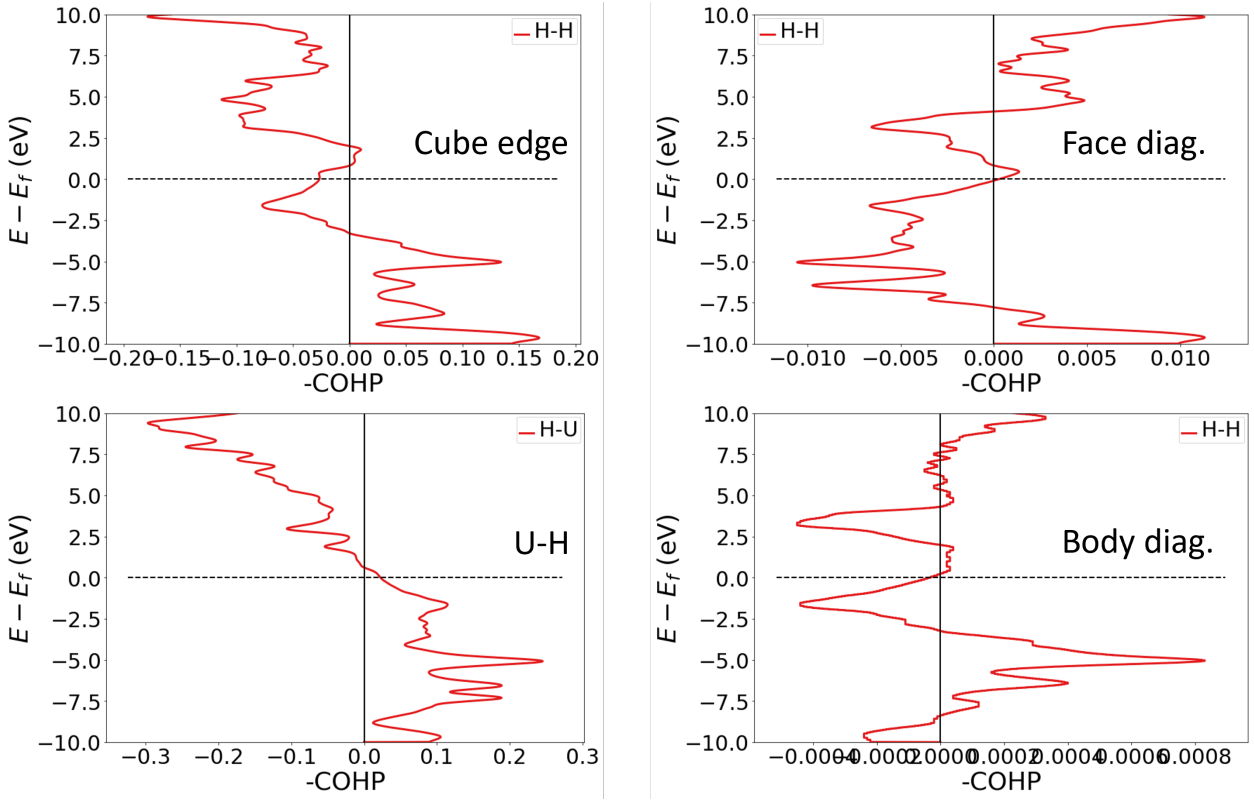

Figure S12: COHP plots for UH_8 at 0 GPa

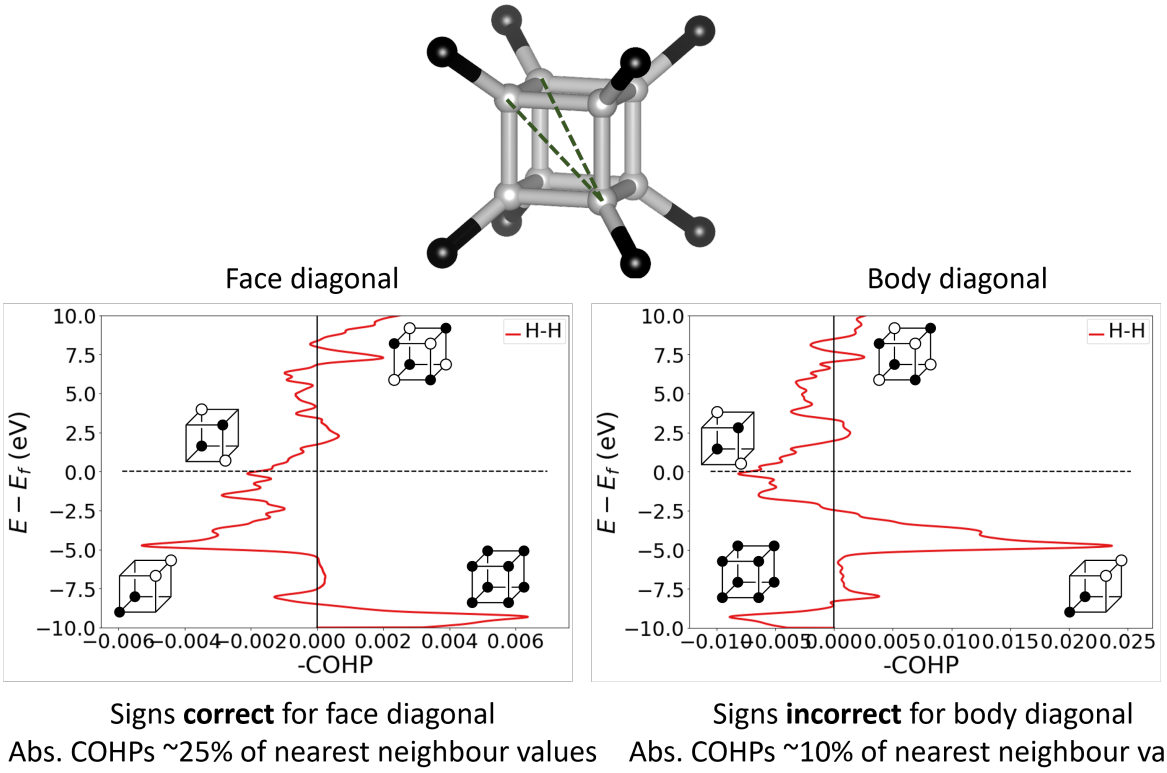

Figure S13: COHPs for H-H pairs along the diagonals of the H_8 cube in LaH_{10} at 0 GPa . Peaks are annotated with corresponding molecular orbital cartoons to show bonding/antibonding relationships.

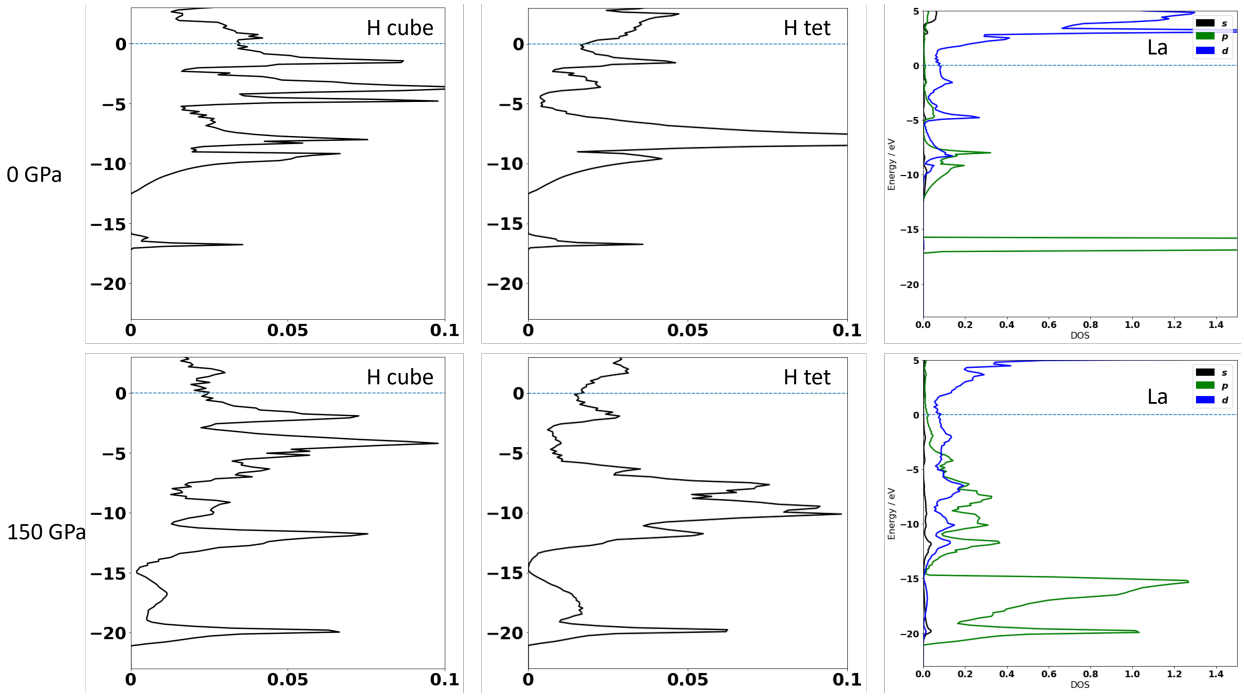

Figure S14: PDOS plots for H (cube), H (tet), and La in LaH_{10} at 0 and 150 GPa (upper and lower rows respectively). The La PDOS is resolved into s (black), p (green), and d (blue) contributions. Increasing pressure from 0 to 150 GPa causes largely uniform broadening of the DOS peaks, but the essential features of each atom and the distinctions between atoms are preserved across the pressure range.

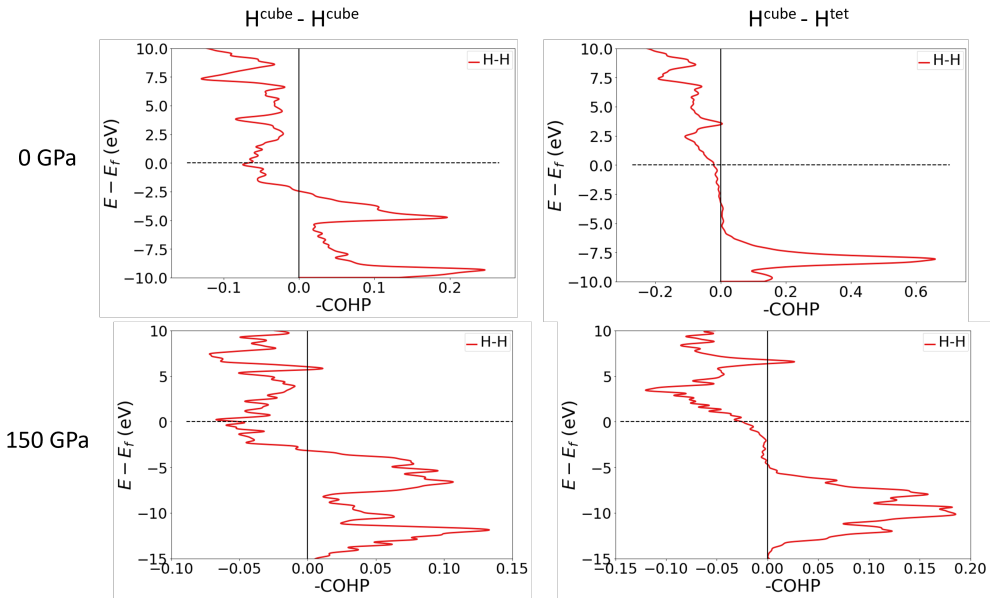

Figure S15: COHP plots for H^{cube} and H^{tet} pairs in LaH_{10} at 0 and 150 GPa. Due to peak broadening under pressure, the 150 GPa plots have a wider energy range than the 0 GPa plots.

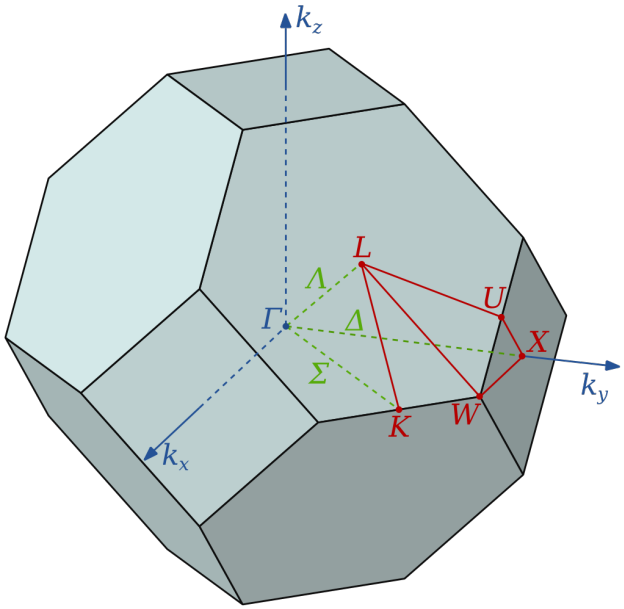

Figure S16: Brillouin zone of $Fm\bar{3}m$-LaH_{10} highlighting high-symmetry k-points. Image source: https://commons.wikimedia.org/wiki/File:Brillouin_Zone_(1st,_FCC).svg